ARTICLE

BIOTECHNOLOGY and BIOENGINEERING

Antifouling Activity of Enzyme-Functionalized Silica Nanobeads

Michele Zanoni, Olivier Habimana, Jessica Amadio, Eoin Casey

School of Chemical and Bioprocess Engineering, University College Dublin, Belfield Dublin 4, Dublin, Ireland; telephone: +353-1-716-1877; fax: +353017161177; e-mail: eoin.casey@ucd.ie

ABSTRACT: The amelioration of biofouling in industrial processing equipment is critical for performance and reliability. While conventional biocides are effective in biofouling control, they are potentially hazardous to the environment and in some cases corrosive to materials. Enzymatic approaches have been shown to be effective and can overcome the disadvantages of traditional biocides, however they are typically uneconomic for routine biofouling control. The aim of this study was to design a robust and reusable enzyme-functionalized nano-bead system having biofilm dispersion properties. This work describes the biochemical covalent functionalization of silica-based nanobeads (hereafter referred to as Si-NanoB) with Proteinase K (PK). Results showed that PK-functionalized Si-NanoB are effective in dispersing both protein-based model biofilms and structurally altering *Pseudomonas fluorescens* biofilms, with significant decreases in surface coverage and thickness of 30.1% and 38.85%, respectively, while increasing surface roughness by 19 % following 24 h treatments on bacterial biofilms. This study shows that enzyme-functionalized nanobeads may potentially be an environmentally friendly and cost effective alternative to pure enzyme and chemical treatments.

Biotechnol. Bioeng. 2016;113: 501–512.

© 2015 The Authors. *Biotechnology and Bioengineering* Published by Wiley Periodicals, Inc.

KEYWORDS: biofilm; enzyme; nanoparticles; antifouling

Introduction

It is generally recognized that the majority of microorganisms found in the natural and technical environments, are present in the form of a biofilm: a multidimensional microbial-ecosystem comprised of a network of aggregated cells attached on either biotic or abiotic surfaces and immobilized by a self-produced matrix of extracellular polymeric substance (EPS) (Flemming and Wingender, 2010; Hori and Matsumoto, 2010; Kaplan et al., 2003). Biofilm formation on surfaces is initiated by bacterial adhesion, in which bacterial cells first consolidate onto surfaces before proliferating into mature biofilms. In essence, life within a biofilm is known to favor bacterial survival against external stresses, (Blauert et al., 2015; DeQueiroz and Day, 2007; Huang et al., 2013). Among these, resistance against antimicrobial agents is considered the hallmark of the biofilm phenotype (Costerton et al., 1999). It is for this reason that biofilms are ubiquitous in nature, adaptable through a variety of environmental conditions, and are highly resistant to antimicrobial agents (DeQueiroz and Day, 2007). Biofouling of industrial processing equipment has been shown to account for increased operational costs associated with pipeline flow blockages (Flemming, 2002; Hall-Stoodley et al., 2004; Winn et al., 2014), and in some cases, biofouling impedes heat transfer rate in heat exchangers (Melo and Flemming, 2010), increase pressure drop in water circuits (Nguyen et al., 2012), increase pumping energy requirements (Bott, 2011), as well as causing material deterioration through Microbial Induced Corrosion (MIC) (Li et al., 2013; Winn et al., 2014).

The EPS-fraction of biofilms, not only offers a continuous source of nutrients to embedded cells, but has also been shown to actively react with antimicrobial agents by slowing their diffusion through the entire biovolume. Among the popular low-cost biofilm amelioration strategies include oxidizing biocides such as chorine or peroxides (Zhang and Hu, 2013). While these are generally effective and have a nonspecific mode of action against biofilms, they are, in general, environmentally unfriendly. One of the most common strategies investigated to address the biofouling problem, is the surface modification of materials (Caruso, 2001) with the intention of improving their resistance to biological adhesion and/or biofilm proliferation (Nuzzo, 2003). This approach is particularly prevalent in the marine industry, with the development of new non-toxic antifouling strategies such as biocidal paints and biomimetic surfaces (Magin et al., 2010).

Since surface coatings and chlorine-based chemical agents are detrimental to the environment due to their leaching properties (Omae, 2003) and bacterial resistance (Brozel et al., 1995), novel "green" antifouling approaches have recently been explored. An original method that paves the way for the preparation of smart-

This is an open access article under the terms of the Creative Commons Attribution-NonCommercial-NoDerivs License, which permits use and distribution in any medium, provided the original work is properly cited, the use is non-commercial and no modifications or adaptations are made.

Michele Zanoni and Olivier Habimana contributed equally to this work.
Correspondence to: E. Casey
Contract grant sponsor: Science Foundation Ireland
Contract grant number: 12/TIDA/B2395
Contract grant sponsor: European Research Council (ERC)
Contract grant number: 278530
Received 3 July 2015; Revision received 24 August 2015; Accepted 7 September 2015
Accepted manuscript online 15 September 2015;
Article first published online 28 September 2015 in Wiley Online Library (http://onlinelibrary.wiley.com/doi/10.1002/bit.25835/abstract).
DOI 10.1002/bit.25835

antifouling nanocomposites is an approach involving Vanadium pentoxide nanowires, presented by Natalio et al. (2012), where V_2O_5 mimics the activity of the naturally occurring enzyme Vanadium peroxidases and forms non-toxic species (such as singlet Oxygen) to reduce bacterial adhesion. Another smart antimicrobial method recently presented, is constituted by nitric oxide-releasing silica nanoparticles (Duong et al., 2014; Hetrick et al., 2009).

Another approach to the biofouling problem is the use of enzymes. In particular (Kristensen et al., 2008), proteases have demonstrated considerable anti-biofilm properties by directly targeting and digesting specific molecules of the biofilm's exopolymeric matrix (Kristensen et al., 2008). Commercialized anti-biofilm products, such as DispersinB^{TM}, which hydrolyses poly-N-acetylglucosamine, have effectively been applied to disperse established biofilms (Brindle et al., 2011; Fazekas et al., 2012; Turk et al., 2013), and also feature as an ingredient in an antibiofilm formula comprised of an array of different enzyme agents among which, Proteinase K (Madhyastha et al., 2009). Although successfully implemented in a medical context of wound healing, the use of such enzymes in a larger industrial context still remains a challenge in part due to the costs associated with enzyme loss and enzyme efficiency. By successfully immobilizing enzymes onto materials that can easily be recovered after use, the use of such immobilized enzymes could be effective for biofilm dispersal in industrial settings in an environmental friendly context. Thus, the design of new nano-materials bearing enzymatic functionalities with biocidal activity is a potentially promising direction (Kristensen et al., 2008; Létant et al., 2004).

Existing enzyme immobilization techniques, which include covalent attachment, entrapment in organic or inorganic matrixes or cross-linking of enzyme molecules (Ariga et al., 2013; Hartmann and Kostrov, 2013; Létant et al., 2004; Li and Wang, 2013; Sheldon, 2007; Wu et al., 2013), all involve the use of different scaffolds. The covalent substitution of enzymes onto a wide range of chemically engineered surfaces, such as magnetic carriers (Yu et al., 2012), hybrid silver-silica nano-composites (Das et al., 2013), or pure silica beads (Kim et al., 2006), has shown to be the most affordable methods to prevent leaching and enzyme loss during multiple-use cycles. A number of bio-inspired silica nanoparticles and nanobeads is reported in the literature (Acosta et al., 2012; Alonso et al., 2005; DiCosimo et al., 2013; Dujardin and Mann, 2002; Guerrero-Martínez et al., 2010; Hartmann and Kostrov, 2013; Montalti et al., 2014; Tang et al., 2012). Their use is supported by versatility and flexibility, by the very broad range of existing chemical functionalization (Li and Wang, 2013; Luckarift et al., 2004). Furthermore, the immobilization of enzymes on silica beads could facilitate the efficient recovery and reuse of otherwise costly proteins.

There is currently a limited understanding of the application of functionalized particles against mature biofilms. Hence the objective of this study was to first synthesize a new class of Silica based nanobeads, hereafter referred to as Si-NanoB, by functionalization with an enzyme known for dispersing biofilms: Proteinase K (PK) (obtained from *Tritirachium album*), and to test their efficiency against model and real biofilms by assessing their combined mechanical and chemical dispersive properties.

Materials and Methods

Materials

Water soluble 1-[3-(dimethylamino) propyl]-3-ethylcarbodiimide hydrochloride (WCA), tetraethylorthosilicate (TEOS), Trimethoxysilylpropyldiethylenetriamine (DETA, a silanization reagent) and succinic anhydride were purchased from Fluorochem Ltd. (Hadfield, United Kingdom). All other chemicals for the buffers, culture broths and solvents were of analytical reagent grade and were purchased from Sigma–Aldrich Co. LLC (Arklow, Ireland). Distilled deionized water was used for the preparation of all solutions, suspensions and buffers. Confocal Microscopy glasses were purchased from Labtek®, Thermoscientific (Waltham MA). Syringe micro filters were purchased from VWR Ltd. (Ireland).

Preparation of Bacterial Suspension

The selected bacterial strain for this study was a mCherry-expressing *Pseudomonas fluorescens* WCS365, was stored at −20°C in King B broth supplemented with 10% glycerol. Cultures were obtained by inoculating 100 mL King B broth supplemented with gentamicin at a final concentration of 10 $\mu g\,mL^{-1}$ using a 1 mL thawed −20°C stock culture. The inoculated medium was then incubated at 28°C with shaking at 75 rpm and left to grow to late exponential growth stages, corresponding to an Optical Densities ($OD_{600\,nm}$) of about 1.0 (a.u.). A 150 mM stock solution of $CaCl_2$ (Sigma–Aldrich), was prepared in MilliQ water, prior to sterilization at 121°C for 15 min. This $CaCl_2$ solution was used to supplement King B broth at a final $CaCl_2$ concentration of 1.5 mM, prior biofilm harvesting experiments.

Synthesis of the Silica Nanobeads (Si-NanoB)

The synthesis of the silica Nanobeads was carried out following the Stöber process (Stoeber et al., 1968). Five hundred microliters (0.466 g, 2.24 mmol) of TEOS were dissolved in 15 mL of pure ethanol (EtOH) in an iced cooled conical flask placed in an ultrasonicator bath (Elma model Elmasonic S40H Ultrasonic Heating Bath). The temperature was kept constant at 0°C for the entire process. Fifteen microliters of 14.5 M NH_4OH (28–30% in NH_3) were slowly added to the reaction mixture during sonication and the reaction was allowed to proceed for 1 h. When the reaction was completed, the nanoparticles were centrifuged and washed thoroughly (3–4 times) with water and acetone and kept in aqueous suspension. Immediately before the functionalization step, the nanobeads were extracted and dried at 60°C for 1 h. The silanization of the nanobeads was obtained in 30 mL of a freshly prepared 1% v/v of DETA dissolved in 1 mM acetic acid solution for 30 min at room temperature. The excess of DETA was removed by rinsing and centrifuging the nanobeads with deionized water for at least 3 times. The silanized nanoparticles were transferred in a sealed conical flask and treated with 30 mL of a 10% w/v succinic anhydride solution in dry Dimethylformammide (DMF) for 6 h under a N_2 atmosphere. The resulting carboxylated beads were extracted from the DMF solution and thoroughly rinsed with deionized water.

Enzyme-Functionalized Silica Nanobeads (Si-NanoB+PK)

The surface activation of the nanobeads with WCA (Water Soluble Carbodiimide) was completed following the Bangs Laboratory protocol (Bangs Laboratories). Following this step, the nanobeads were suspended in aqueous PBS (pH 7.4) and concentrated to a 100 mg mL^{-1} suspension. Proteinase K (PK, 1 mg mL^{-1}) was added to the suspension and the mixture was allowed to react for 24 h at 25°C. According to our analysis (Sigma Aldrich), the amount of enzyme detected for each milligram of lyophilized powder received from the producer is 0.74 mg mL^{-1}. The enzyme-functionalized nanobeads were finally washed with deionized water through three centrifugation steps at 5000 rpm at room temperature before storage at 4°C in PBS (pH 7.4). The yield of the reaction was quantified by the Proteinase K enzymatic protocol that can be found on the Sigma Aldrich website (Sigma Aldrich).

Characterization of the Silica Nanobeads

Silanized silica nanobeads and enzyme-functionalized silica nanobeads were characterized by:

- Scanning electron microscopy (SEM): for scanning electron microscopy (SEM) observations, silica nanobeads suspensions of 10 mg mL^{-1} were dried on stubs at 60°C overnight prior to gold sputtering using an Eintech K575K coater for 30 s at 30 mA. High magnification imaging of non- functionalized and functionalized silica nanobeads was performed under a Hitachi Quanta 3D FEG scanning electron microscope at the UCD Nano-imaging and Materials Analysis Centre.
- Flow cytometry: to further assess the structural differences between non-functionalized and functionalized silica nanobeads, the Accuri™ C6 flow cytometer was employed to reveal the size and inner complexities between the different silica nanobeads used in this study. Analysis was based on light scatter signals produced from 20 mW laser illumination at 488 nm. Signals corresponding to forward angle and 90°—side scatter (FALS, SS) were accumulated. Threshold levels were empirically set (80000 for FALS) to eliminate the detection of irrelevant debris. Templates for uni- and bi-parametric frequency distributions were established of the region corresponding to silica nanobeads, and the data collected to total of 50000 events. The flow cytometry routine was operated at a slow flow rate setting (0.6 μL sample/second).
- FTIR: FTIR measurements were obtained with a Varian 680 FTIR (Agilent Technologies Ltd., Cork, Ireland) instrument. The samples were oven-dried at 40°C, after this they were individually casted on AFM-Grade bare Mica (Novascan Technologies, Inc., Ames, IA) and immediately analyzed.
- X-ray Photon Spectroscopy (XPS): The surface elemental compositions of the modified silica beads were determined using Kratos Axis Ultra XPS system, Kratos Analytical Ltd. (Manchester, United Kingdom). Excitation X-rays were produced by a monochromatic Al K α1,2 source, with a takeoff angle of 90°. Wide scans were performed to analyze all existing elements on the silica beads surfaces and high-resolution narrow scan analysis was performed for peak deconvolution of carbon C1s, nitrogen N1s, oxygen O1s and silica Si2p signals. All binding energies were referenced to the C1s hydrocarbon peak at 285.0 eV.
- Dynamic Light Scattering (DLS): particle size and polydispersity of the beads were assessed by dynamic light scattering. The measurements were obtained with a Zetasizer Nano-ZS Nano series (Malvern Instruments, Malvern, United Kingdom). After their synthesis, the samples were suspended in PBS (pH 7.4) and a 1 mL aliquot was placed inside a disposable capillary cell (DTS1070, Malvern Instruments Ltd.) for the analysis. The analysis of each of the two samples was repeated in triplicate.

Preparation of the artificial biofilm (protein hydrogel): The artificial biofilm was prepared by suspending in 100 mL of deionized water under stirring equal amounts (8 g) of vegetable Peptone, Albumin and Agar. The pH of the suspension was adjusted to 3 with a 0.1 M HCl solution and the mixture was stirred for 30 min at room temperature. In order to analyze the gels with the Confocal Microscopy, aliquots of 2 mL of the mixture were placed in individual Labtek® well chambers which were then transferred into an incubator at 60°C for 2 h for gelification.

Preparation of *Pseudomonas fluorescens* Biofilms

A 5 μL volume of an overnight culture of *P. fluorescens* (adjusted to $OD_{600nm} = 1.2$ abs) was used to inoculate sterile individual centrifuge tubes (Falcon, Fischer scientific, Dublin, Ireland) each containing 3 mL King B broth supplemented with gentamicin (10 μg mL^{-1} final concentration) and $CaCl_2$ (1.5 mM final concentration). Single autoclaved cover slips (Thermo Scientific, Germany, borosilicate glass 18 × 24 mm), were partially submerged into individual tubes. Individual 10 mL tips were used for stabilizing the glass slide inside each tube, before sealing each tube with sterile cotton wool. The tubes were then incubated for 24 h at 28°C with shaking at 75 rpm.

Quantification of the Enzyme-Functionalized Silica Nanobeads Activity

Prior to assays, 10 mg mL^{-1} of either non-functionalized and functionalized Si-NanoB were suspended in a specific reaction buffer (30 mM Tris Cl, 30 mM EDTA, 10 mM $CaCl_2$ and a 0.5% aliquot of Triton-X100) previously prepared in deionized water and stored between 2 and 8°C.

- Artificial biofilm: Three gels were individually prepared following a method previously reported (Strathmann et al., 2000) with minor modifications: the gels were composed of a cocktail of different proteins (albumin and soy proteins) and polysaccharides (including agar) to reproduce the roughness of a typical biofilm. Artificial biofilms were prepared in an aqueous medium used for gelification, adjusted to pH 3 using 0.1 M HCl. The acidic conditions facilitated the gelification of the system. The final formulation (Figure S4(a)) was chosen because of its adaptability and reproducibility closely matching the chemical composition of a typical bacteria-based biofilm. Furthermore, the ease of preparation, the capacity to mold the gel structure and the availability of the ingredients used in preparation of the gel, allowed a reliable and fast production of the different

substrates for each analysis. Treatment assays consisted of submerging single protein hydrogels with 5 mL of either reaction buffer solution, non-functionalized silica nanobeads (1 mg mL^{-1}) or functionalized silica nanobeads (1 mg mL^{-1}), before incubation at 25°C for 24, 48, and 72 h with shaking at 75 rpm. Following each treatment period, gels were stained with 20 μL of Albumin 580 blue dye for 1 h prior to confocal microscopy observations. Experiments were repeated in triplicates.

- *Pseudomonas fluorescens* biofilm: Following 24 h growth at 28°C, coverslips containing confluent biofilms were initially dipped in sterile saline water (100 mM NaCl) for rinsing, before being individually placed at the bottom of small petri dishes, each containing 5 mL of either reaction buffer solution, non-functionalized silica nanobeads (10 mg mL^{-1}) or functionalized silica nanobeads (10 mg mL^{-1}). Once submerged, biofilms were then treated at 28°C with shaking set to 75 rpm for 24 h. At the end of each 24 h treatments, biofilms were dipped in sterile saline water for rinsing before being at the bottom of single-well Nunc® Lab-Tek® II Chamber Slide™ (VWR, Ireland) previously filled with sterile saline water, which were then observed and analyzed trough confocal microscopy. Experiments were performed in duplicates using two independently grown cultures.
- Confocal microscopy: Horizontal plane images of the biofilms were acquired using an Olympus FV1000 confocal laser-scanning microscope (CLSM) at the Live Cell Imaging core technology facility platform, Conway Institute, UCD. At least 2–3 random areas were acquired for each treated artificial biofilm and biofilm per experiment. The excitation wavelength used for detecting Albumin 580 blue or mCherry was 559 nm, and emitted fluorescence was recorded within the range of 570–670 nm. Images were collected through an Olympus UPL SAPO 10x/0.40 Air objective with a z-step of 1 μm. 3D projections were performed with Zeiss ZEN imaging software. The structural quantification of biofilms (biovolume, surface coverage, thickness and roughness) was performed using the PHLIP Matlab program developed by J. Xavier (http://phlip.sourceforge.net/phlip-ml). (Mueller et al., 2006)

The statistical significance of differences in the treatment efficiency between the different Silica Nanobeads on either artificial biofilms or *P. fluoresens* biofilms was assessed using one-way analysis of variance with MINITAB v15.1 (Minitab Inc., State College, PA). Statistical differences in biovolume quantities (μm3), surface coverage (%), mean thickness (μm), and biofilm roughness of artificial biofilms and *P. fluorescens* biofilms treated with Si-NanoB and Si-NanoB+PK were analyzed with Tukey's test for pair wise comparisons. All tests were performed at a 5% significance level.

Recovery of the Functionalized Silica Nanobeads

Si-NanoB and Si-NanoB+PK were collected following each treatment assay. Collection of Si-NanoB+PK was also performed following biofilm-rinsing steps. In order to keep the sterility of the recovered beads, Si-NanoB+PK were filtered through sterile 0.45 μm syringe filters, which were separately rinsed and cleaned using sterile deionized water in a laminar flow hood through several centrifugation-washing steps. Recovered silica nanoparticles were stored in sterile PBS (pH 7.4) at 2–8°C.

Results and Discussion

Synthesis of Enzyme-Functionalized Silica Nanobeads

The Si-NanoB were synthesized following a general method already available from the literature (Stoeber et al., 1968). The beads were functionalized with PK, which was selected for its broad range of activity against various biomolecules in environmental conditions as well as for its ease of covalent attachment on the nano-carriers.

These surfaces can easily be modified with different reagents in mild conditions for a high variety of applications. The major modification mechanisms used in this work are presented in Figure S1. This procedure is based on the creation of primary amine functional groups onto the particle silica surface, which are then treated with succinic anhydride. In order to host covalent bonds with PK, the nanobeads were carboxylated prior to enzyme immobilization. PK (dissolved in PBS, 1 mg mL^{-1}) immobilization to nanobeads was performed by first incubating the particles in PBS with the pH adjusted to 6.8 for 24 h at 25°C under stirring, according to the procedure reported by Bangs Laboratories (TechNote 205, Bangs Laboratories). The quantity of enzyme covalently bound to the beads was calculated following the method reported by Cantarero (Cantarero et al., 1980), which indicates that ~32 mg of pure proteinase K are necessary to saturate 1 g of silica nanobeads having a 500 nm diameter. However, since the purity of the samples of proteinase K obtained was 0.74 mg of enzymes per mg of lyophilized powder, the quantity of proteinase K that was covalently bound to the Si-NanoB was calculated to be 6.95 mg of enzyme per gram of Si-NanoB, as evidenced by the calculated reaction yield (94% [±0.9%]). The quantity of unreacted enzyme determined in the post-reaction solution obtained after several washing steps in PBS was found to be 6% (±0.24 %), as monitored by recording the maximum absorbance at 450 nm as directed by the Proteinase K assay (Sigma Aldrich).

As reported in a number of previous studies, the activity of some particular biomolecules such as cytochromes and specific enzyme families when immobilized onto solid supports is stabilized and in some cases even enhanced (Hanefeld et al., 2009; Hartmann and Kostrov, 2013; Shang et al., 2009). However, Shang et al. (2007) recently suggested that the size of the nanobeads can negatively influence the activity of the enzyme immobilized on an inert surface. Nevertheless, from a general point of view, the method chosen for the attachment of the enzyme is a crucial step in the preparation of the bioactive beads; in this study, covalent functionalization was the preferred method over the other chemical and physical techniques, in order to increase and improve the stability of the enzyme (Hartmann and Kostrov, 2013). This paves the way for the development of a number of possible applications for similar beads for antibacterial applications.

Characterization of the Enzyme Grafted Silica Nanobeads

XPS-spectroscopy measurements were performed to determine the surface elemental compositions of the prepared silica nanobeads.

Table I. Elemental analyses of (a) Si-NanoB and (b) Si-NanoB+PK obtained using XPS with a takeoff angle of 90°.

Element	Positive (eV)	Atomic conc (%)	Mass conc (%)
	Si-NanoB		
C 1s C-C	284.557	27.3	21.02
C 1s C-N, C-O	286.06	16.17	12.45
C 1s C-Ox	287.462	2.46	1.89
O 1s C-O	530.789	6.54	6.7
O 1s Si-O	532.283	28.58	29.3
O 1s C-Ox	533.194	3.39	3.48
Si 2p	103.017	12.41	22.33
N 1s	399.443	3.15	2.83
	Si-NanoB+PK		
C 1s C-C	284.522	40.43	35.68
C 1s C-N, C-O	286.022	15.59	13.76
C 1s C-Ox	287.679	9.66	8.53
O 1s C-O	531.166	8.26	9.71
O 1s Si-O	532.56	13.8	16.23
O 1s C-Ox	533.556	3.64	4.28
Si 2p	103.516	2.84	5.87
N 1s	399.511	5.78	5.94

The results are summarized in Table I and presented in Figure 1. The chemical bonds of the base material surfaces were investigated by deconvolution of the C1s carbon peaks, performed according to previous reports (Nagase et al., 2014; Nagase et al., 2012). The XPS peaks of the non-functionalized Si-NanoB surfaces (Si-NanoB, Fig. 1a) were different from those of the Si-NanoB+PK, Figure 1b. Specifically, the spectra of the Si-NanoB+PK displayed an additional peak at 286 eV, which corresponds to the C═O bonds of the enzyme (PK); this was also confirmed by an increased amount of the signal at 399 eV for the Si-NanoB+PK sample, which indicates an increased abundance of nitrogen belonging to the enzyme. Furthermore, as expected, the silicon content decreased and the carbon and nitrogen contents increased after the enzyme reaction because an enzyme layer covered the silica surfaces. These XPS measurements suggested that the enzyme was successfully grafted on the Si-NanoB surfaces.

FTIR-spectroscopy was employed as a means to assess and verify the successful immobilization and presence of PK on functionalized Si-NanoB. Acquired FTIR spectra were compared with spectra of non-functionalized Si-NanoB (Figure S2). Spectral differences between functionalized and non-functionalized Si-NanoB were noticeable, clearly indicating the presence of the enzyme on the surface of the materials studied. For reference, the main spectra assignments are presented in Table S1, in which the most important identified functional units, indicating the presence of immobilized enzyme, are highlighted in bold.

To qualitatively assess the morphological state of Si-NanoB, two samples of the functionalized and non-functionalized nanobeads were synthesized with the previously described procedure and dried at 50°C for the analysis with scanning electron microscopy (SEM), Figure S3(a–d). Both series of micrographs suggested that the beads are spherical and monodispersed. In particular, Si-NanoB (Figure S3(a and b)) appeared relatively smooth and presented a well-defined shape while Si-NanoB+PK (Figure S3(c and d)) appeared rougher and heterogeneous (d). The size of the two different classes of nanobeads was estimated by dynamic light scattering (DLS): the non-functionalized beads had a hydrodynamic diameter of 501 nm (±40 nm), meanwhile the hydrodynamic diameter of the Si-NanoB+PK increased by ∼100 nm to 638 nm (±25 nm). As desired, the DLS returned purified particles with an average size of ∼500 nm, which is 5 times larger than what reported previously (∼100 nm, according to Qhobosheane et al.) (Peulen and Wilkinson, 2011; Qhobosheane et al., 2001). The particle size in the present study was chosen, in part, to provide a mechanical ablation action against biofilms. Since the presence or absence of PK on the surface of Si-NanoB is the most important difference, the likelihood of the observed surface disparities between tested samples and an averaged difference of ∼100 nm between the non-functionalized and the enzyme-functionalized beads, can be ascribed by the physical presence of the PK enzymes on the nanobeads' outer surface.

Artificial Biofilm: Qualitative Results

It is widely accepted that the biofilm EPS matrix offers protection to its embedded microorganisms. The chemical characterization of the biofilm matrix is complicated by the wide variation in composition of EPS synthesized by the organisms, which is usually strain dependent and influenced by the environmental conditions in which the biofilm is grown (Wolfaardt et al., 1999). The use of a reproducible artificial biofilm model of a known chemical composition is a useful system to facilitate the screening and optimization antibiofilm strategies. In the present study the artificial biofilm was used as a preliminary screening step for assessment of enzyme-functionalized nanobeads (Peulen and Wilkinson, 2011; Wolfaardt et al., 1999).

To assess the specific role and activity of non-functionalized and Si-NanoB+PK, a standardized artificial biofilm (Figure S4) matrix was employed to monitor both the mechanical and enzymatic properties of the Si-NanoB. The use of such artificial biofilms for mimicking complex biofilm systems has been described elsewhere (Hellriegel et al., 2014).

The performance of functionalized and non-functionalized Si-NanoB (1 mg mL^{-1}) in terms of removal of artificial biofilms following 24, 48, and 72 h treatments at 25°C is shown in Figures 2 and 3a–d. The treated gels were analyzed using confocal microscopy and compared to gels treated in either buffer (control a) or in a solution of PK (control b). At shown in Figure 2b and d there is significant structural changes for the artificial biofilms, in terms of cluster formation, when treated with PK in solution or with Si-NanoB+PK respectively. In contrast, no such clusters were observed following the treatment using Si-NanoB (Fig. 2c). Furthermore, the density of these clusters for gels treated with Si-NanoB+PK (Fig. 2d) can be seen to decrease over the course of 72 h, thereby hinting at probable digestion from this particular treatment. The combined effect of Si-NanoB+PK (Fig. 2d) was shown to have inflicted more damage to the artificial biofilm compared to any of the previous treatments, as observed by the level of gel disintegration. The results shown in Figure 2 are qualitative and it was therefore necessary to undertake quantitative assessment of the different treatment types.

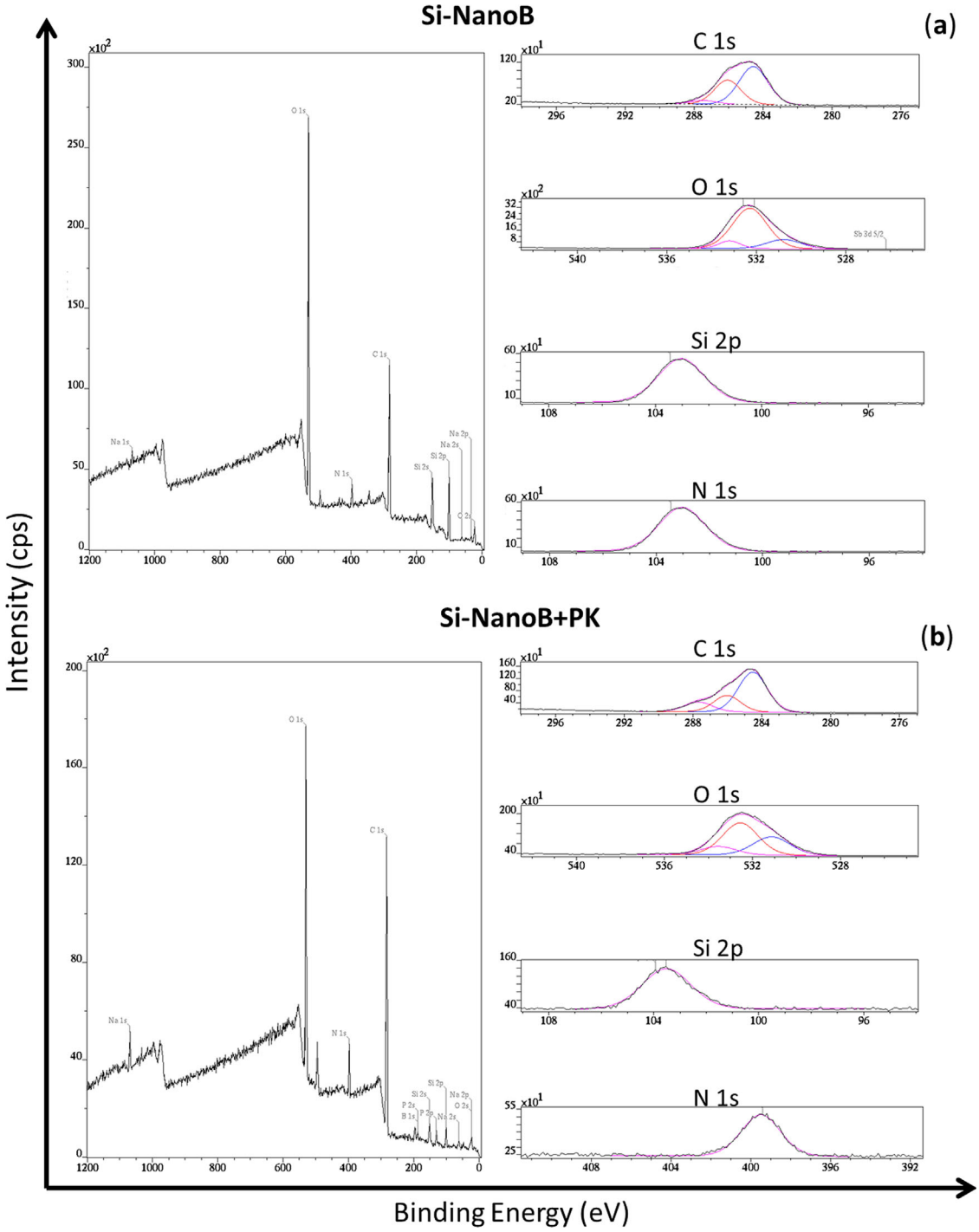

Figure 1. XPS micrographs of (**a**) Si-NanoB and (**b**) Si-NanoB+PK.

Artificial Biofilm: Quantitative Results

The combined qualitative (Fig. 2a–d) and quantitative (Fig. 3a–d) results obtained with CLSM show that the coupling of both nanobeads and enzymes has the potential to disintegrate the gel structure. The degree of gel structural changes following the different treatment types were quantitatively analyzed using acquired confocal images with PHLIP image analysis (Mueller et al., 2006). This software allows quantification of biofilm structure from CLSM data via statistical analysis of the data sets collected. Specifically its outputs include: biovolume (volume of cells in a unitary amount of water, μm^3), mean thickness (μm), surface coverage (percentage of removed biofilms from the substrate) and roughness (intended as the number of irregularities or

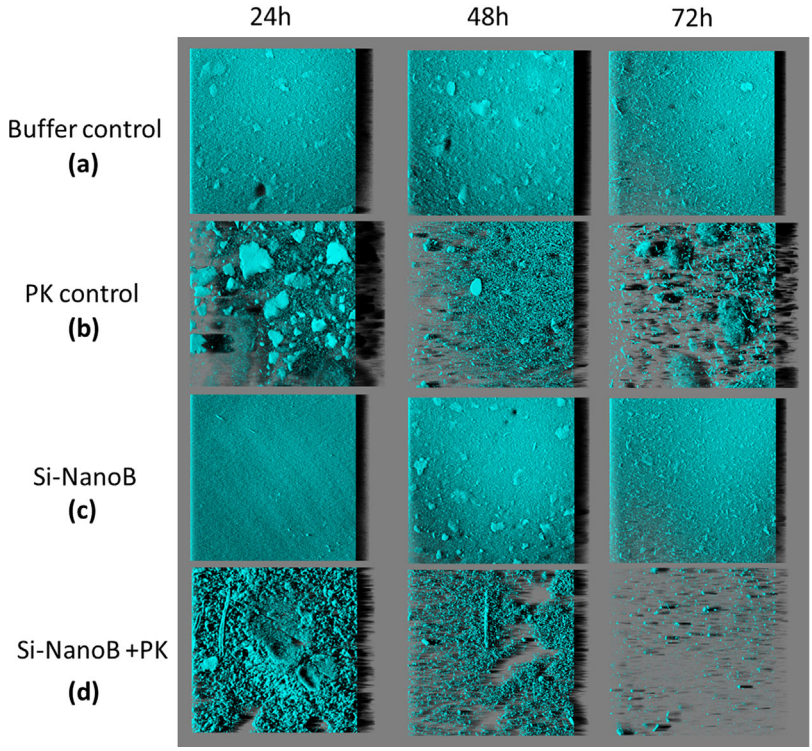

Figure 2. Confocal micrographs of protein–based hydrogels treated for 24, 48, and 72 h with buffer control solution (**a**), PK buffer control (**b**), Si-NanoB (**c**), and Si-NanoB+PK (**d**).

breaks observed on the biofilms), Figure 3a–d. The effects of Si-NanoB+PK on the artificial biofilm over the course of the 24, 48, and 72 h treatments, was clearly observed by the significant reduction in biovolume ($P = 0.0234$), surface coverage ($P = 0.0025$) and thickness ($P = 0.0039$) of the artificial biofilm compared to the artificial biofilms treated with control solutions. In the case of Si-NanoB+PK, a high biovolume observed after 24 h treatment (Fig. 3a) could be explained by the presence of gel clumps in the liquid suspension ablated by Si-NanoB+PK. The lower biovolume measured after the 48 and 72 h experiments confirm the successful enzymatic action of the Si-NanoB+PK. No particular effect was observed for Si-NanoB when compared to buffer control treatments, as seen by the resulting biovolume ($P = 0.4333$), surface coverage ($P = 0.5279$), mean thickness ($P = 0.6648$) or gel surface roughness ($P = 0.3839$) following 72 h treatment. Interestingly, artificial biofilms treated with PBS buffered solution do not present the same degree of structural change compared to gels treated with Si-NanoB+PK, as observed by an unaltered biovolume ($P = 0.5261$), or mean thickness ($P = 0.0631$) over the course of the treatment. The sole use of enzyme solution (PK control) was found to only have decreased gel surface coverage ($P = 0.0157$) and increased gel surface roughness ($P = 0.0341$) over the course of the 72 h treatment. This clearly shows active capacity of the free enzyme in solution, which was able to diffuse through the artificial biofilm and react with the proteins within the gel matrix. In contrast, the combined action of Si-NanoB+PK not only caused structural damage to the artificial biofilm as can be seen from a smaller substrate coverage (Fig. 3c) and by a higher gel roughness (Fig. 3d), but also through the increased reactive surface action, was capable of digesting larger portions of the gel. This observed double-action of Si-NanoB+PK was found to be the ideal combination to successfully remove the artificial biofilm.

Activity of Recycled Nanobeads After 24, 48, and 72 h

In order to assess the reusability of Si-NanoB+PK, they were studied over 3 different recycling treatments. Standardized artificial biofilm were treated at 25°C with either freshly prepared Si-NanoB and Si-NanoB+PK or recycled Si-NanoB and Si-NanoB+PK (cf. supplementary Figures S5 and S6) for 24, 48, and 72 h. The presence and the activity of the enzyme on the recovered Si-NanoB+PK were assessed by the PK enzymatic assay already described in the material and methods section and by flow cytometry (see Figure S5 (a–c)). As control treatments, artificial biofilms were exposed to either a buffer (PBS pH 7.4) or PK buffer solutions for the same treatment period. Confocal microscopy analyses were performed following treatments, allowing qualitative assessments of the treatment effects on the artificial biofilms (see Figure S6(a–f)).

Compared to fresh Si-NanoB+PK, recycled nanobeads generally showed reduced mechanical or enzymatic activity on the artificial biofilms. Although the nanobeads were washed during the recycling steps, it is very likely that some remnant materials from previously treated gels may have possibly covered the recovered beads. Optimizing the activity of recycled nanobeads for subsequent treatment used should therefore focus on the development of alternative and highly efficient recovery and cleaning

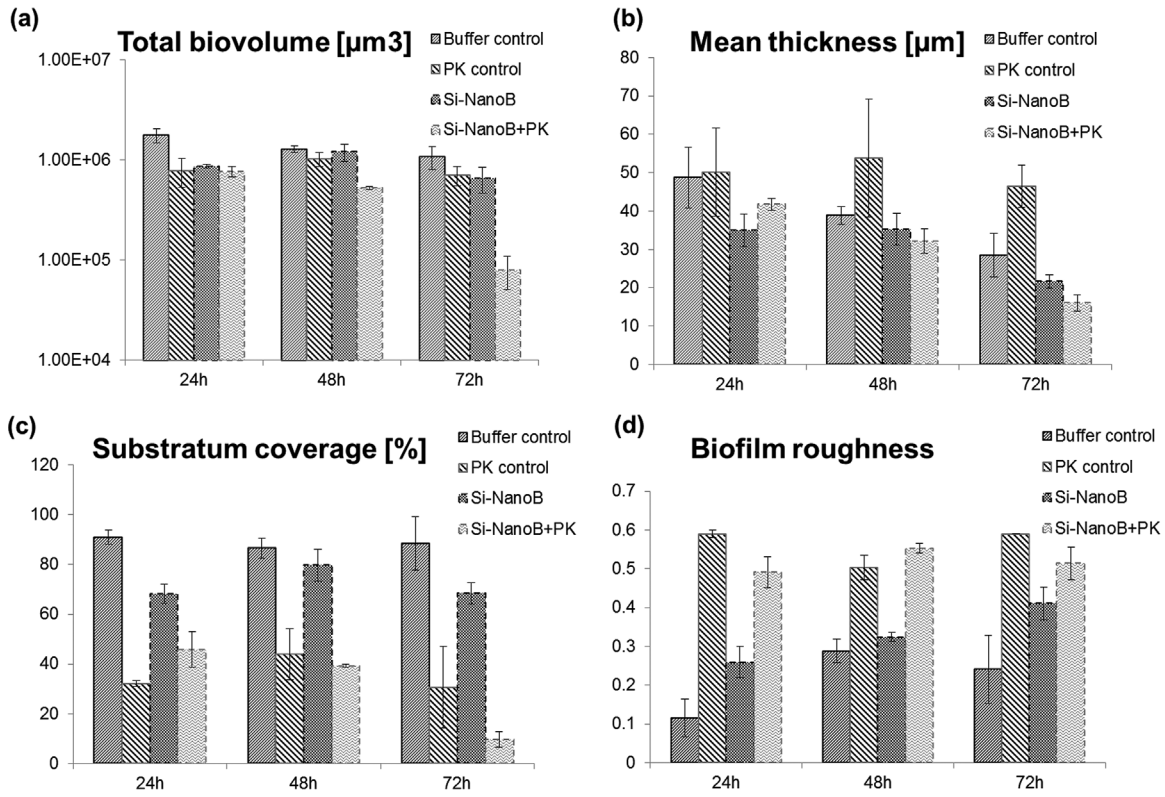

Figure 3. Structural properties of protein-based hydrogels following 24, 48, and 72 h treatment with buffer control, PK buffer control, Si-NanoB, or Si-NanoB+PK. Structural hydrogel properties were obtained following PHLIP analysis and are presented in terms of biovolume (**a**), substratum coverage (**b**), mean thickness (**c**) and roughness (**d**).

methodologies that would fully preserve their functional properties of the beads following multiple operational cycles.

Concentration-Dependent Activity of Si-NanoB+PK Over 24 h

To investigate the degree of activity on the artificial biofilms, 24 h treatment assays were performed using two sets of Si-NanoB concentrations, high and low, corresponding to 10 mg mL^{-1} and 0.1 mg mL^{-1} of nanobeads in suspension, respectively. The structural properties of the artificial biofilms following Si-NanoB treatments were compared using low or high concentrations of either Si-NanoB or Si-NanoB+PK during treatment (Figure S7). Increasing the concentration of Si-NanoB did not increase the level of mechanical damage compared to lower concentrations of Si-NanoB as observed by the structural properties analysis of treated gels. Interestingly, increasing the concentration of Si-NanoB+PK led to significant changes to the artificial biofilm structure, as seen by the reduced biovolume, substratum coverage, thickness parameters and increased roughness when comparing to treatments at lower Si-NanoB concentrations.

Si-NanoB+PK Application on Real Biofilm: *Pseudomonas fluorescens* Biofilms

After gaining understanding of the activity of functionalized nanobeads on artificial biofilms, the efficacy of Si-NanoB+PK was tested on live biofilm systems. Two sets of experiments were performed in which *P. fluorescens* biofilms were treated, respectively, with a buffer control, Si-NanoB and with Si-NanoB+PK.

Since this experiment was intended to validate the potential activity of the nanobeads against bacterial-generated biofilms, a standard treatment time was arbitrarily set at 24 h according to the previously reported catalytic performances studied for the PK (Ebeling et al., 1974). Qualitative assessments were performed on treated biofilms following treatments using CLSM microscopy (Fig. 4a–c). The degree of biofilm removal following treatment was also quantified by performing PHLIP analysis on acquired CLSM data (Table II) (See Figure S8(a–c)). Although biofilms are complex and heterogeneous in nature, Si-NanoB+PK treatments (Fig. 4c) appear to have induced structural damage to the biofilms.

The analysis of the 24 h experiments revealed that the mechanical damage produced by Si-NanoB on *P. fluorescens* was not relevant in terms of biovolume ($P = 0.9572$), surface coverage ($P = 0.5497$), mean thickness ($P = 0.8847$), and biofilm roughness ($P = 0.9517$) when compared to the control. However, in comparison to buffer samples, Si-NanoB+PK led to a 30.1% drop in surface coverage ($P = 0.03$), 38.8% drop in thickness ($P = 0.002$) and a 19% increase in biofilm roughness ($P = 0.01$) following a 24 h treatment period. No significant differences were observed in biovolume between biofilms treated between the Si-NanoB+PK and buffer treated samples ($P = 0.1275$).

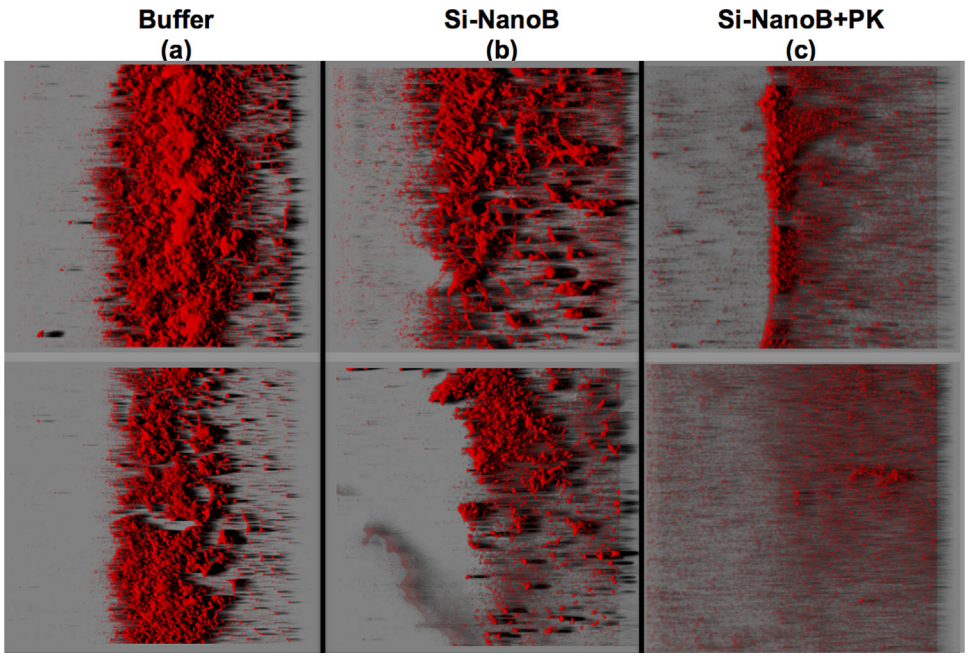

Figure 4. Confocal micrographs of mCherry-tagged *P. fluorescens* biofilms treated for 24 h with buffer solution (**a**), Si-NanoB (**b**), or Si-NanoB+PK (**c**).

The different efficiency of Si-NanoB+PK on such complex structures compared to the results obtained on the artificial biofilms could be attributed to the intrinsic biofilm composition. While the studied artificial gel mimicked biofilm EPS matrix, the real biofilms included bacterial cells. The insignificant change in biofilm biovolume in this study shows that the 24-treatment did not affect the number of cells within the biofilm. However, significant changes in surface coverage, thickness and roughness during treatment, suggests that Si-NanoB+PK was able to alter the organization of cells within biofilms, by targeting key proteins with the biofilm EPS matrix. Regardless of the level of treatment efficiency, this study was still able to show that functionalized nanobeads were capable of provoking significant structural alteration of biofilms, which may be optimized to facilitate the removal of bacterial cells by either introducing a flushing mechanisms or by applying a secondary antibacterial treatment aimed at efficiently eliminating newly released planktonic cells. The latter strategy would be preferential since cells within biofilms are offered better protection from antibacterial agents owing to the presence of a complex EPS matrix capable of either neutralizing the antibacterial agents or limiting its ability to diffuse through the biofilm EPS matrix (Stewart, 1996). Moreover, the elimination of released cells would also inhibit any subsequent re-colonization and biofilm formation on new surfaces.

Although potentially efficient in provoking structural damage against biofilms, the enzymatic action of Si-NanoB+PK on *P. fluorescens* biofilms still needs to be improved. Admitting that the 24 h treatment period can be considered as lengthy, from an industrial perspective in the context of Cleaning In Place (CIP) operations, the success of the proof-of-concept study presented here forms the basis for further optimization, which could include the functionalization of additional enzymes and different treatment periods under different dynamic environments defined by the presence of shear conditions.

Biofilm Removal: Post Treatment Analysis of Bulk Suspension

Bulk suspension samples were analyzed using flow cytometry following 24 h biofilm treatment with buffer, Si-NanoB and Si-NanoB+PK. This analysis is widely applied for cell counting, for cell sorting and for biomarker detection and it was applied in this study to further characterize and confirm the anti-biofilm action of Si-NanoB and the results are depicted in Figure 5. Prior to each

Table II. Quantification parameters following 24 h biofilm treatment with buffer, Si-NanoB and Si-NanoB+PK on *P. fluorescens* biofilms using PHLIP analysis of acquired CLSM data. Error represents standard error of the mean.

	Buffer	Si-NanoB	Si-NanoB-PK
Total biovolume [μm^3]	127552.04 ± 11046.95	144134.4 ± 52753.3	92114.48 ± 20510.2
Substratum coverage [%]	13.6 ± 1.3	12.30 ± 3.5	9.50 ± 1.9
Mean thickness [μm]	32.68 ± 2.1	33.90 ± 1.9	19.99 ± 2.1
Biofilm roughness	0.38 ± 0.01	0.38 ± 0.06	0.44 ± 0.08

analysis, the samples were marked with 10 μL of a stock solution of Concanavalin A (conA), a member of the family of the lectins, which becomes fluorescent (emission at 594 nm) upon complexing glucopyranosyl derivatives contained in biological samples; the detection by flow cytometry of these luminescent complexes allowed the statistical quantification of the components released by the biofilm during the treatment. Compared to biofilms treated in buffer, the presence of Si-NanoB particles during treatment led to an incremented granularity of detached clumps as observed by the increased Side Scatter Area data (Fig. 5a). This mechanical ablation was not fully observed during CLSM analysis but it may indicate that this typology of nanobeads has a dual-activity mechanism of action against biofilms. This increase was more pronounced when using Si-NanoB+PK compared to the other treatments studied. These results suggest that the state and structure of detached cells from biofilms is linked to the type of treatment used. Biofilms treated with buffer resulted in the release of cells in a highly compact state whereas the mechanical action of Si-NanoB led to a looser and disintegrated state of detached cells, which was amplified in the presence of an enzymatic reaction.

This hypothesis was further corroborated when analyzing the mCherry fluorescence intensity profiles of the bulk liquid samples (Fig. 5b). Compared to buffer treated samples, the fluorescence intensity profiles of the studied bulk suspension following Si-NanoB treatments led to a decrease in mCherry positive fluorescence events. Moreover, treatment-using Si-NanoB+PK, led to even fewer mCherry positive fluorescence events compared to treatment using Si-NanoB. This further shows that the mechanical and enzymatic actions of the tested Si-NanoB+PK did contribute in altering the state of detached cells during biofilm treatment. This was further demonstrated by analyzing the carbohydrate fraction of detached EPS of the bulk suspension following the nanobeads activity (Fig. 5c). Samples collected from buffer-treated biofilms revealed a low detection of conA positive counted events, which could have been the result of reduced dye reactivity caused by the smaller surface area of detached cells.

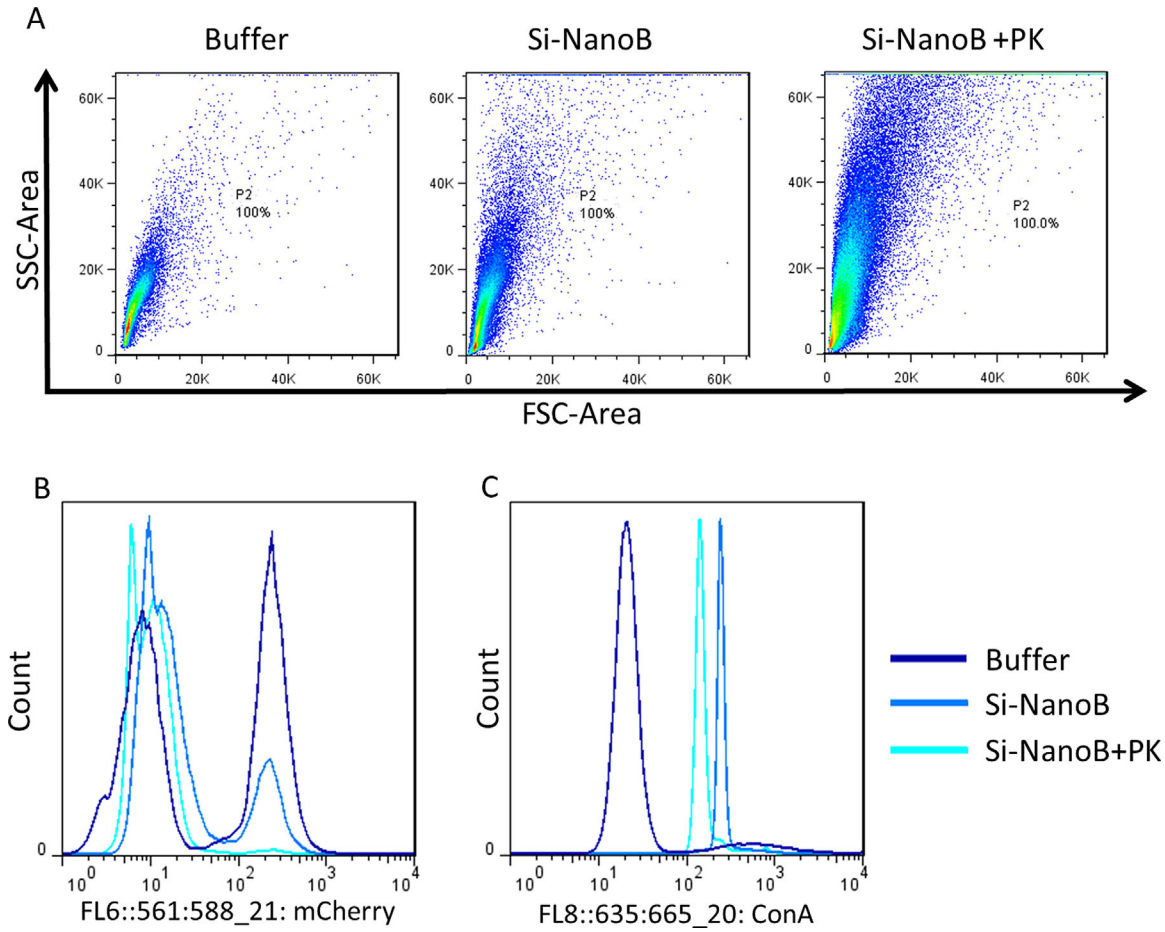

Figure 5. Bulk suspension analysis following 24 h treatment using Buffer, Si-NanoB and Si-NanoB+PK on mature *P. fluorescens* biofilms. (**A**) Representative plots depicting gated elements based on side scatter-area and forward scatter-area for the morphological description of the bulk suspension following biofilm treatment. Each dot represents a measured event; its position indicates its forward scatter (FSC) intensity value (event size), and its side scatter (SSC) intensity value (event granularity). (**B**) Representative histograms characterizing the presence of mCherry expressing *P. fluorescens* cells and (**C**) the fraction of stained carbohydrate components of biofilm EPS following treatment using a conA lectin dye. The events are distributed within the histogram based on detected signal intensity. Events emitting a stronger signal are assigned to the higher channels along the x-axis, while dimmer events are located in the lower channels.

Higher conA positive counted events following of bulk suspension samples with Si-NanoB treatment, suggests that the mechanical action of the Si-NanoB led to an increase in surface area, as well as an increased exposure of carbohydrate components of detached EPS, which was otherwise not detected from confocal analysis of the residual biofilm. This result places an emphasis on investigating bulk liquid samples following biofilm treatment, which may help better understand the antifouling properties of a given type of treatment. Interestingly, a noticeable reduction in conA positive fluorescence intensity signal was observed for samples collected following the exposure to the Si-NanoB+PK compared to treatment using Si-NanoB. This suggests that the enzymatic reaction of Si-NanoB+PK targeting proteins in the EPS matrix might have led to a structural alteration of the EPS matrix, by reducing its overall size and composition, which in the process reduced the fraction of detectable carbohydrates and subsequent fluorescence intensity.

These results show that treating biofilms with Si-NanoB+PK not only led to successful mechanical detachment of biofilms, but also proved to be an efficient means of dispersing detached cells. This is especially significant in terms of devising novel strategies in biofilm treatment in which dispersed cells following Si-NanoB+PK action can subsequently be eliminated in synergy with antimicrobials.

Conclusions

In summary, the surface of silica-based nanobeads was functionalized with Proteinase K enzyme (Si-NanoB+PK) through covalent binding; these bioactive carriers were tested on two different systems: an artificial biofilm (model biofilm) and a biofilm of *P. fluorescens*. Despite the relatively prolonged treatment duration, the Si-NanoB+PK beads were shown to be an efficient biofilm-dispersal agent where the biochemical action of the enzyme is efficiently combined to the mechanical activity of the silica core. The chemical stabilization of the enzyme supplied by the covalent substitution on the beads surface allowed the successful recovery of the used beads following biofilm dispersal. Such functionalized nanobeads paves the way for the identification of a new family of non-corrosive and environmentally friendly anti-biofilm and antifouling agents. Si-NanoB+PK recovery consisted of several sequences of combined filtration and washings, which were shown to have minimal effect on their specific activity. This strategic advantage opens up a promising approach for the synthesis of a wide range of similar derivatives bearing similar anti-bacterial activity, in which their ease of recovery coupled with the re-usable properties would enable the more cost effective use of enzyme based cleaning operations in industry. Future perspectives should therefore focus on optimizing the enzymatic actions of nano-carriers for enhanced biofilm dispersal properties by targeting the various proteins, polysaccharides, and lipids, which usually make up the biofilm matrix.

This research was supported by Science Foundation Ireland under grant number 12/TIDA/B2395. Additional support was provided by the European Research Council (ERC), project 278530, funded under the EU Framework Program 7. The authors would like to thank Dr. Ian Reid of the NIMAC microscopy platform UCD, Dr. Alan Casey from DIT and Ms. Ashley Allen for their assistance with XPS-spectroscopy, dynamic light scattering (DLS) and scanning electron microscopy (SEM) and Dr. Alfonso Blanco-Fernandez of the Conway Institute Flow Cytometry Core facility. The authors especially thank Dr. Ellen L. Lagendijk from the Institute of Biology Leiden, Netherlands, for the gift of the mCherry-tagged *Pseudomonas fluorescens* PCL 1701 strain. The authors declare no conflicting interests.

Electronic Supplementary Information (ESI) available: chemical functionalization of the nanobeads; FTIR spectra and assignments; SEM images of the Silica nanobeads; images of the artificial biofilm; recycled nanobeads activity tests; concentrated versus diluted activity of the nanobeads; Si-NanoB+PK application on real biofilm.

References

Acosta MA, Velasquez M, Williams K, Ross JM, Leach JB. 2012. Fluorescent silica particles for monitoring oxygen levels in three-dimensional heterogeneous cellular structures. Biotechnol Bioeng 109(10):2663–2670.

Alonso B, Clinard C, Durand D, Veron E, Massiot D. 2005. New routes to mesoporous silica-based spheres with functionalised surfaces. Chem Comm (13):1746–1748.

Ariga K, Ji Q, Mori T, Naito M, Yamauchi Y, Abe H, Hill JP. 2013. Enzyme nanoarchitectonics: Organization and device application. Chem Soc Rev 42(15):6322–6345.

Bangs Laboratories I. 9025 Technology Drive Fishers, IN 46038-2866, USA, 1-800-387-0672.

Blauert F, Horn H, Wagner M. 2015. Time-resolved biofilm deformation measurements using optical coherence tomography. Biotechnol Bioeng 112(9): 1893–1905.

Bott TR. 2011. Chapter 7—biofilms in industry. In: Bott TR, editor. Industrial biofouling. Amsterdam: Elsevier. p 181–201.

Brindle ER, Miller DA, Stewart PS. 2011. Hydrodynamic deformation and removal of Staphylococcus epidermidis biofilms treated with urea, chlorhexidine, iron chloride, or DispersinB. Biotechnol Bioeng 108(12):2968–2977.

Brozel V, Pietersen B, Cloete TE. 1995. Resistance of bacterial cultures to non-oxidising water treatment bactericides by adaptation. Water Sci Technol 31(5):169–175.

Cantarero L, Butler J, Osborne J. 1980. The adsorptive characteristics of proteins for polystyrene and their significance in solid-phase immunoassays. Anal Biochem 105(1):375–382.

Caruso F. 2001. Nanoengineering of particle surfaces. Adv Mater 13(1):11–22.

Costerton JW, Stewart PS, Greenberg EP. 1999. Bacterial biofilms: A common cause of persistent infections. Science 284(5418):1318–1322.

Das SK, Khan MMR, Parandhaman T, Laffir F, Guha AK, Sekaran G, Mandal AB. 2013. Nano-silica fabricated with silver nanoparticles: Antifouling adsorbent for efficient dye removal, effective water disinfection and biofouling control. Nanoscale 5(12):5549–5560.

DeQueiroz GA, Day DF. 2007. Antimicrobial activity and effectiveness of a combination of sodium hypochlorite and hydrogen peroxide in killing and removing *Pseudomonas aeruginosa* biofilms from surfaces. J Appl Microbiol 103(4):794–802.

DiCosimo R, McAuliffe J, Poulose AJ, Bohlmann G. 2013. Industrial use of immobilized enzymes. Chem Soc Rev 42(15):6437–6474.

Dujardin E, Mann S. 2002. Bio-inspired Materials Chemistry. Adv Mater 14(11):775–788.

Duong HTT, Jung K, Kutty SK, Agustina S, Adnan NNM, Basuki JS, Kumar N, Davis TP, Barraud N, Boyer C. 2014. Nanoparticle (star polymer) delivery of nitric oxide effectively negates *Pseudomonas aeruginosa* biofilm formation. Biomacromolecules 15(7):2583–2589.

Ebeling W, Hennrich N, Klockow M, Metz H, Orth HD, Lang H. 1974. Proteinase K from Tritirachium album Limber. Eur J Biochem 47(1):91–97.

Fazekas E, Kandra L, Gyémánt G. 2012. Model for β-1, 6-N-acetylglucosamine oligomer hydrolysis catalysed by DispersinB, a biofilm degrading enzyme. Carbohydr Res 363:7–13.

Flemming H-C. 2002. Biofouling in water systems-cases, causes and countermeasures. Appl Microbiol Biotechnol 59(6):629–640.

Flemming H-C, Wingender J. 2010. The biofilm matrix. Nat Rev Microbiol 8(9): 623–633.

Guerrero-Martínez A, Pérez-Juste J, Liz-Marzán LM. 2010. Recent progress on silica coating of nanoparticles and related nanomaterials. Adv Mater 22(11): 1182–1195.
Hall-Stoodley L, Costerton JW, Stoodley P. 2004. Bacterial biofilms: From the natural environment to infectious diseases. Nat Rev Microbiol 2(2):95–108.
Hanefeld U, Gardossi L, Magner E. 2009. Understanding enzyme immobilisation. Chem Soc Rev 38(2):453–468.
Hartmann M, Kostrov X. 2013. Immobilization of enzymes on porous silicas—benefits and challenges. Chem Soc Rev 42(15):6277–6289.
Hellriegel J, Günther S, Kampen I, Bolea Albero A, Kwade A, Böl M, Krull R. 2014. A biomimetic gellan-based hydrogel as a physicochemical biofilm model. J Biomater Nanobiotechnol 5:83–97.
Hetrick EM, Shin JH, Paul HS, Schoenfisch MH. 2009. Anti-biofilm efficacy of nitric oxide-releasing silica nanoparticles. Biomaterials 30(14):2782–2789.
Hori K, Matsumoto S. 2010. Bacterial adhesion: From mechanism to control. Biochem Eng J 48(3):424–434.
Huang Z, McLamore ES, Chuang HS, Zhang W, Wereley S, Leon JLC, Banks MK. 2013. Shear-induced detachment of biofilms from hollow fiber silicone membranes. Biotechnol Bioeng 110(2):525–534.
Kaplan JB, Ragunath C, Ramasubbu N, Fine DH. 2003. Detachment of Actinobacillus actinomycetemcomitans biofilm cells by an endogenous β-hexosaminidase activity. J Bacteriol 185(16):4693–4698.
Kim J, Grate JW, Wang P. 2006. Nanostructures for enzyme stabilization. Chem Eng Sci 61(3):1017–1026.
Kristensen JB, Meyer RL, Laursen BS, Shipovskov S, Besenbacher F, Poulsen CH. 2008. Antifouling enzymes and the biochemistry of marine settlement. Biotechnol Adv 26(5):471–481.
Létant SE, Hart BR, Kane SR, Hadi MZ, Shields SJ, Reynolds JG. 2004. Enzyme immobilization on porous silicon surfaces. Adv Mater 16(8):689–693.
Li K, Whitfield M, Van Vliet KJ. 2013. Beating the bugs: Roles of microbial biofilms in corrosion. Corros Rev 31(3–6):73–84.
Li Ll, Wang H. 2013. Enzyme-coated mesoporous silica nanoparticles as efficient antibacterial agents in vivo. Adv Healthc Mater 2(10):1351–1360.
Luckarift HR, Spain JC, Naik RR, Stone MO. 2004. Enzyme immobilization in a biomimetic silica support. Nat Biotechnol 22(2):211–213.
Madhyastha S, Gawande P, Lovetri K, Yakandawala N, Kaplan JB. 2009. Dispersinb tm, 5-fluorouracil, deoxyribonuclease i and proteinase k-based antibiofilm compositions and uses thereof. Google Patents.
Magin CM, Cooper SP, Brennan AB. 2010. Non-toxic antifouling strategies. Mater Today 13(4):36–44.
Melo LF, Flemming HC. 2010. Mechanistic aspects of heat exchanger and membrane biofouling and prevention. The science and technology of industrial water treatment A.Z. Talyor and Francis Group: Florida.
Montalti M, Prodi L, Rampazzo E, Zaccheroni N. 2014. Dye-doped silica nanoparticles as luminescent organized systems for nanomedicine. Chem Soc Rev 43(12):4243–4268.
Mueller LN, De Brouwer JF, Almeida JS, Stal LJ, Xavier JB. 2006. Analysis of a marine phototrophic biofilm by confocal laser scanning microscopy using the new image quantification software PHLIP. BMC Ecol 6(1):1.
Nagase K, Kobayashi J, Kikuchi A, Akiyama Y, Kanazawa H, Okano T. 2014. Monolithic silica rods grafted with thermoresponsive anionic polymer brushes for high-speed separation of basic biomolecules and peptides. Biomacromolecules 15(4), 1204–1215.
Nagase K, Mukae N, Kikuchi A, Okano T. 2012. Thermally Modulated Retention of Lymphoctytes on Polymer-Brush-Grafted Glass Beads. Macromol Biosci 12(3):333–340.
Natalio F, André R, Hartog AF, Stoll B, Jochum KP, Wever R, Tremel W. 2012. Vanadium pentoxide nanoparticles mimic vanadium haloperoxidases and thwart biofilm formation. Nat Nanotech 7(8):530–535.
Nguyen T, Roddick FA, Fan L. 2012. Biofouling of water treatment membranes: A review of the underlying causes, monitoring techniques and control measures. Membranes 2(4):804–840.
Nuzzo RG. 2003. Biomaterials: Stable antifouling surfaces. Nature Mater 2(4):207–208.
Omae I. 2003. General aspects of tin-free antifouling paints. Chem Rev 103(9):3431–3448.
Peulen T-O, Wilkinson KJ. 2011. Diffusion of nanoparticles in a biofilm. Environ Sci Technol 45(8):3367–3373.
Qhobosheane M, Santra S, Zhang P, Tan W. 2001. Biochemically functionalized silica nanoparticles. Analyst 126(8):1274–1278.
Shang W, Nuffer JH, Dordick JS, Siegel RW. 2007. Unfolding of Ribonuclease A on Silica Nanoparticle Surfaces. Nano Lett 7(7):1991–1995.
Shang W, Nuffer JH, Muñiz-Papandrea VA, Colón W, Siegel RW, Dordick JS. 2009. Cytochrome c on silica nanoparticles: Influence of nanoparticle size on protein structure, stability, and Activity. Small 5(4):470–476.
Sheldon RA. 2007. Enzyme immobilization: The quest for optimum performance. Adv Synth Catalysis 349(8-9):1289–1307.
Sigma Aldrich I. http://www.sigmaaldrich.com/technical-documents/protocols/biology/enzymatic-assay-of-proteinase-k1-hemoglobin-substrate.html, corrected.
Stewart PS. 1996. Theoretical aspects of antibiotic diffusion into microbial biofilms. Antimicrob Agents Chemother 40(11):2517–2522.
Stoeber W, Fink A, Bohn E. 1968. Controlled growth of monodisperse silica spheres in the micron size range. J Colloid Interf Sci 26(1):62–69.
Strathmann M, Griebe T, Flemming HC. 2000. Artificial biofilm model—a useful tool for biofilm research. Appl Microbiol Biotechnol 54(2):231–237.
Tang F, Li L, Chen D. 2012. Mesoporous silica nanoparticles: Synthesis, biocompatibility and drug delivery. Adv Mater 24(12):1504–1534.
Turk R, Singh A, Rousseau J, Weese JS. 2013. In vitro evaluation of DispersinB on methicillin-resistant Staphylococcus pseudintermedius biofilm. Vet Microbiol 166(3):576–579.
Winn M, Casey E, Habimana O, Murphy CD. 2014. Characteristics of Streptomyces griseus biofilms in continuous flow tubular reactors. FEMS Microbiol Lett 352(2):157–164.
Wolfaardt G, Lawrence J, Korber D. 1999. Function of EPS. In: Wingender J, Neu T, Flemming H-C, editors. Microbial extracellular polymeric substances. Berlin, Heidelberg: Springer. p 171–200.
Wu S, Buthe A, Jia H, Zhang M, Ishii M, Wang P. 2013. Enzyme-enabled responsive surfaces for anti-contamination materials. Biotechnol Bioeng 110(6): 1805–1810.
Yu C-C, Kuo Y-Y, Liang C-F, Chien W-T, Wu H-T, Chang T-C, Jan F-D, Lin C-C. 2012. Site-specific immobilization of enzymes on magnetic nanoparticles and their use in organic synthesis. Bioconjug Chem 23(4):714–724.
Zhang Y, Hu Z. 2013. Combined treatment of *Pseudomonas aeruginosa* biofilms with bacteriophages and chlorine. Biotechnol Bioeng 110(1):286–295.

Supporting Information

Additional supporting information may be found in the online version of this article at the publisher's web-site.